Letter

Pinch-off of viscoelastic particulate suspensions

Virgile Thiévenaz [®] and Alban Sauret ^{®†}
Department of Mechanical Engineering, University of California, Santa Barbara, California 93106, USA



(Received 12 February 2021; accepted 3 May 2021; published 4 June 2021)

The formation of drops of a complex fluid, for instance including dissolved polymers and/or solid particles, has practical implications in several industrial and biophysical processes. In this Letter, we experimentally investigate the generation of drops of a viscoelastic suspension, made of non-Brownian spherical particles dispersed in a dilute polymer solution. Using high-speed imaging, we characterize the different stages of the detachment. Our experiments show that the particles primarily affect the initial Newtonian necking by increasing the fluid viscosity. In the viscoelastic regime, particles do not affect the thinning until the onset of the blistering instability, which they accelerate. We find that the transition from one regime to another, which corresponds to the coil-stretch transition of the polymer chains, strongly depends on the particle content. Considering that the presence of rigid particles increases the deformation of the liquid phase, we propose an expression for the local strain rate in the suspension, which rationalizes our experimental results. This method could enable the precise measurement of local stresses in particulate suspensions.

DOI: 10.1103/PhysRevFluids.6.L062301

Many industrial processes and natural phenomena involve the fragmentation of a fluid into droplets [1–4]. For applications as diverse as inkjet printing, bioprinting, and other droplet deposition techniques [5–8], as well as in the study of airborne disease transmission [9,10], the fluid is often complex, loaded with particles, bubbles, cells, as well as dissolved polymers or proteins. The heterogeneity and the granularity of complex fluids lead to a complex rheology. Commonly, such real-life fluids exhibit viscoelasticity, as in polymer solutions, which for instance can be used in living tissue engineering [6], and coating layers of photovoltaic panels [11]. Past studies have mostly considered the formation of droplets from homogeneous fluids, both Newtonian and non-Newtonian [2,12–16], and the influence of a dispersed phase—such as solid particles—remains poorly quantified. In particular, the interplay between a non-Newtonian interstitial fluid with suspended particles remains elusive.

The formation of drops of suspensions is expected to be primarily influenced by the rheology of the interstitial fluid and by the properties of particles. For simple flows of spherical particles that remain small compared to the length scale of the flow, increasing the solid volume fraction ϕ is known to increase the shear viscosity η [17,18]. However, rheology becomes a tricky problem for more complex types of deformations such as the elongational flows encountered during drop formation. The size of the particles also plays a role when it is comparable to the scale of the flow [19–29]. This necessarily happens during drop detachment [30] since the thickness of the liquid neck eventually vanishes. Different studies with non-Brownian, Newtonian suspensions have revealed that in the first moments of the detachment of a pendant drop, the evolution of the minimum diameter of the neck h_{\min} evolves as in the case of a pure homogeneous fluid having the same

^{*}virgile@vthievenaz.fr

[†]asauret@ucsb.edu

effective viscosity as the suspension, independently of the particle size [30–36]. Then, when h_{\min} falls below a certain limit that depends on the particle size and the solid fraction, the thinning accelerates because of discrete particulate effects [37].

The pinch-off of a viscoelastic fluid, such as a polymer solution, is more complex because the thinning involves additional elastic forces [38,39]. At the time when the liquid should break up, the polymer opposes the rupture with an elastic stress. The neck then turns into a filament that stretches as the polymer chains are elongated in the extensional flow. Then, the minimum diameter h_{\min} decreases exponentially [40], whereas for a Newtonian fluid, its decay would follow a power law [41]. This thinning experiment constitutes a classical method for quantifying the viscoelasticity of the liquid since it enables a direct measurement of the polymer characteristic time λ_0 , which translates the relaxation of the elastic strain when the applied stress is released [38,42,43]. The addition of particles modifies the local viscous stress acting on the polymer chains, and thus the rheology of the viscoelastic fluid. Since the filament becomes vanishingly small, discrete particulate effects are expected to play a role on the thinning dynamics and on the final breakup into satellite droplets. However, these couplings remain unknown. The goal of this Letter is to describe and clarify the interplay between the viscoelasticity and dispersed particles.

The suspensions used in this study consist of solid particles dispersed in a viscoelastic interstitial liquid at a volume fraction ϕ . The spherical and monodisperse polystyrene particles (Dynoseeds TS from Microbeads) have a density $\rho_p \simeq 1057 \text{ kg m}^{-3}$, and we used batches of different diameters d ranging from 20 to 140 μ m. The viscoelastic interstitial fluid is a mixture of water (74%), glycerol (25%), and polyethylene oxide (1%) with a molar weight of 300 kg/mol (PEO, from Sigma Aldrich) whose density matches that of the particles. To quantify the effect of the heterogeneities brought by the particles, we also performed experiments using equivalent fluids with larger glycerol concentrations [44]. Their composition is chosen so that their shear viscosity matches that of a suspension of volume fraction ϕ_{eq} [26,32]. The pinch-off experiment consists in slowly extruding the suspension through a nozzle of outer diameter $h_0 = 2.75$ mm using a syringe pump (KDS Legato 110). Outside the nozzle, a pendant drop swells and eventually detaches under its own weight. The thinning dynamics are recorded at 10 000 fps using a high-speed camera (Phantom VEO 710L) equipped with a macrolens (Nikon 200mm f/4 AI-s Micro-NIKKOR) and a microscope lens (Mitutoyo X2). The drop and the neck are backlit with a light-emitting diode (LED) panel (Phlox) to clearly distinguish its contour, which we detect using the software IMAGEJ and a custom-made routine.

Figures 1(a)-1(c) show examples of the evolution of the liquid neck that connects the drop to the nozzle for three different configurations: particle-free interstitial liquid [Fig. 1(a)], 20- μ m particles [Fig. 1(b)], and 140- μ m particles [Fig. 1(c)]. In the two last cases, the solid volume fraction is $\phi = 40\%$. Each series of pictures begins when the neck is 1 mm thick. The pictures on the left show the neck in the Newtonian regime at early times, whereas the pictures on the right show the *filament* in the viscoelastic regime at late times. The transition between one regime to the other occurs at time t_c . In the following, we define the origin of time at $t = t_c$ so that $t - t_c = 0$ corresponds to the transition between the two regimes. In the pure liquid case, shown in Fig. 1(a), the neck quickly thins down and turns into a *filament*, which keeps thinning down until it breaks. The whole process takes a few tens of milliseconds. Shortly before the breakup, the filament undergoes a blistering instability which produces several tiny droplets [45]. Adding $\phi = 40\%$ of 20- μ m particles dispersed in the polymer solution yields a similar behavior in the Newtonian regime, as shown in Fig. 1(b). However, the presence of particles also disturbs and accelerates the blistering, with the droplets now encapsulating particles. A similar dynamic is observed with the larger $140-\mu m$ particles reported in Fig. 1(c). In this last case, the particles deform the free surface from the beginning of the viscoelastic regime, and the destabilization of the filament is even faster.

Let us first compare the thinning of the viscoelastic suspensions to that of the particle-free viscoelastic liquids. Figure 2(a) reports the thinning dynamics $h_{\min}(t)$ for a suspension containing $\phi = 30\%$ of 20- μ m particles, which is compared to the dynamics of the sole interstitial fluid and to that of the equivalent fluid with the same shear viscosity as the suspension. The Newtonian necking

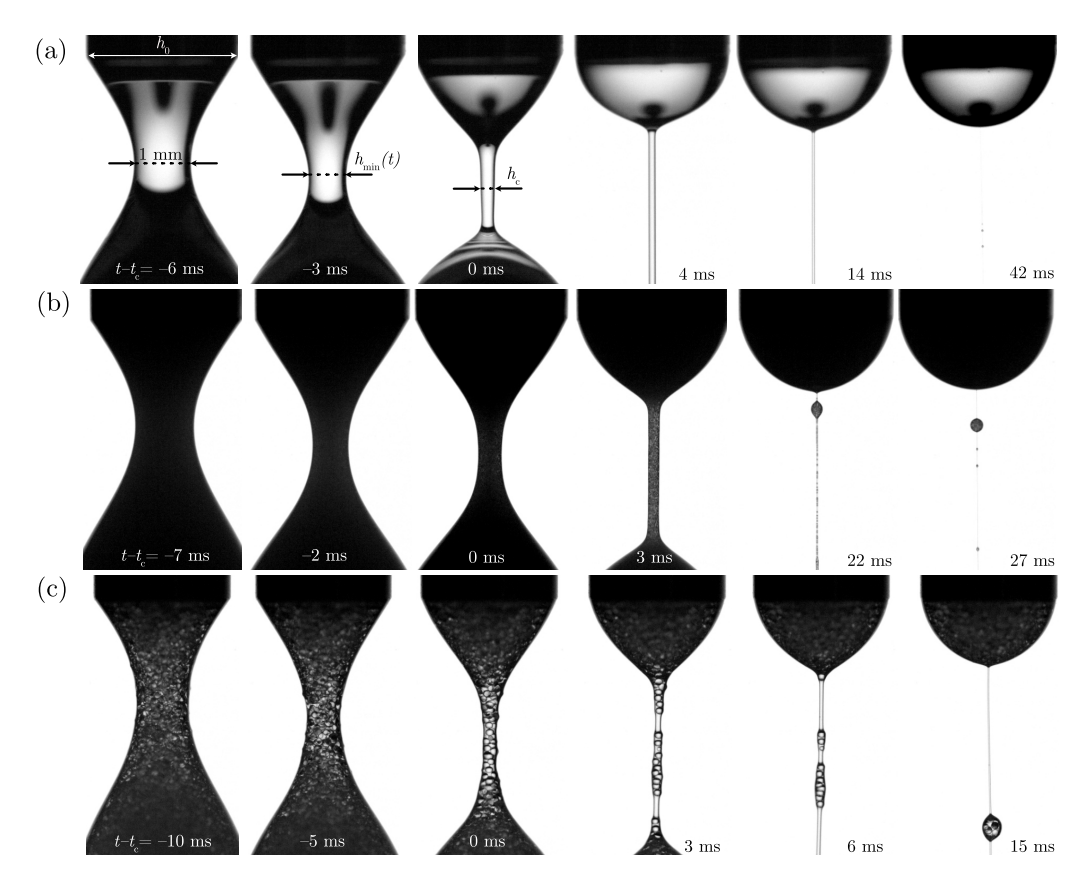


FIG. 1. Detachment of drops of a viscoelastic liquid (74% water, 25% glycerol, 1% PEO300) with and without particles. In the first picture of each row, the neck width is 1 mm. The time stamps display the time to the viscoelastic transition $t-t_c$. (a) Polymer solution only, (b) $\phi=40\%$ of particles of diameter $d=20~\mu\text{m}$, and (c) $\phi=40\%$ of particles of diameter $d=140~\mu\text{m}$.

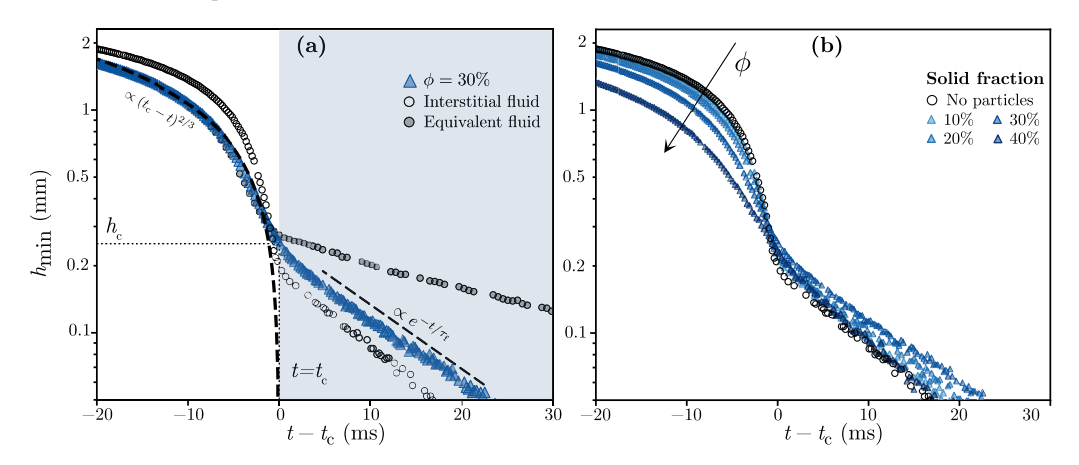


FIG. 2. (a) Thinning dynamics for $\phi=30\%$ of $d=20~\mu\mathrm{m}$ particles compared to the behavior of the interstitial fluid (open circles) and of the equivalent viscous fluid (solid circles). The dashed curve before $t=t_{\rm c}$ shows the capillary-inertial regime $h\propto (t_{\rm c}-t)^{2/3}$ [Eq. (1)], and the dashed line after $t=t_{\rm c}$ shows the viscoelastic regime $h\propto e^{-t/\tau_{\rm f}}$ [Eq. (2)]. (b) Thinning dynamics for different solid volume fractions ϕ of 20- μ m particles.

regime is controlled by the balance between inertia and the surface tension γ . The Ohnesorge number Oh = $\eta_0/\sqrt{\rho\gamma h_0}$, which compares the viscosity of the interstitial fluid η_0 to the inertial and capillary effects, equals 5×10^{-3} for the interstitial fluid. Hence, in first approximation, viscosity should be negligible. Dimensional analysis leads to the scaling law for the time evolution of the diameter at the neck h_{\min} , during the Newtonian regime [46]:

$$h_{\rm min} \propto \left[\gamma (t_{\rm c} - t)^2 / \rho \right]^{1/3}$$
.

We match this scaling law to our experiments using the fitting parameter A, which quantifies the thinning rate in the Newtonian regime:

$$h_{\min} = A(t_{\rm c} - t)^{2/3}$$
. (1)

Equation (1) is plotted in Fig. 2(a) and captures all of our experiments, regardless of the volume fraction and the diameter of the particles dispersed in the viscoelastic liquid phase. This result demonstrates that the Newtonian regime is mostly driven by capillarity and inertia. The critical time t_c is measured from the fitted curve. If there were no polymer chains to inhibit the pinch-off, the finite-time singularity would occur at $t = t_c$ [12]. In the present case, $t = t_c$ is the moment of the transition to the viscoelastic regime. At later stages, the thinning is controlled by the elongational viscosity of the liquid which increases as h_{\min} decreases, because the polymer chains stretch. Therefore, the filament thickness decreases exponentially [40],

$$h_{\min} \propto e^{-t/\tau_{\rm f}},$$
 (2)

where $\tau_f = 3\lambda_0$ is the characteristic decay time of the filament and λ_0 the longest relaxation time of the dissolved polymer chains [47].

As shown in Fig. 2(a), in the Newtonian regime, the viscoelastic suspension (in blue) thins down slower than the pure interstitial fluid (open circles). It follows, however, the exact same dynamics as the equivalent fluid, which matches its shear viscosity. This suggests that although the good fit of Eq. (1) shows a first-order inertial-capillary mechanism, viscosity plays a second-order, yet non-negligible, role. However, we observe that in the viscoelastic regime, the long thread of suspension thins down as fast as the interstitial fluid, much faster than the equivalent viscous fluid. This means that the particles have little or no effect on the long-term stretching of the polymer chains. Figure 2(b) compares the thinning dynamics for different volume fractions of particles ϕ and confirms these trends. In the Newtonian regime, the more particles, the more viscous the suspension, the slower the thinning. In the viscoelastic regime, there is no noticeable effect of the volume fraction of particles. Surprisingly, the thinning dynamics remains that of the sole interstitial viscoelastic liquid.

Fitting Eqs. (1) and (2) to the experiments leads to two physical quantities, A and τ_f , which respectively quantify the thinning rate in the Newtonian and in the viscoelastic regime. Figure 3(a) shows the value of the prefactor A used in Eq. (1) when varying the volume fraction ϕ of the suspension for various particle sizes and for the equivalent viscous fluids. When ϕ is increased, the prefactor A decreases—by a third between $\phi = 0\%$ and $\phi = 30\%$. Since the equivalent viscous fluids behave likewise, this suggests that A captures the amplitude of the second-order effect of viscosity on the thinning. Another way to consider this viscous effect is to see it as a delay of the transition to the viscoelastic regime. Indeed, Eq. (1) can be nondimensionalized into

$$\frac{h_{\min}}{h_0} = A \frac{t_c^{2/3}}{h_0} \left(1 - \frac{t}{t_c} \right)^{2/3}.$$
 (3)

The inset in Fig. 3(a) shows that the rescaled prefactor $A t_c^{2/3}/h_0$ is constant for all experiments performed in this study. The constant value of $A t_c^{2/3}/h_0$ means that viscosity affects the Newtonian thinning regime by changing its timescale. Hence, the thinning dynamic is that of an inviscid fluid subject to inertia and capillarity, but the timescale over which it takes place varies slightly with the

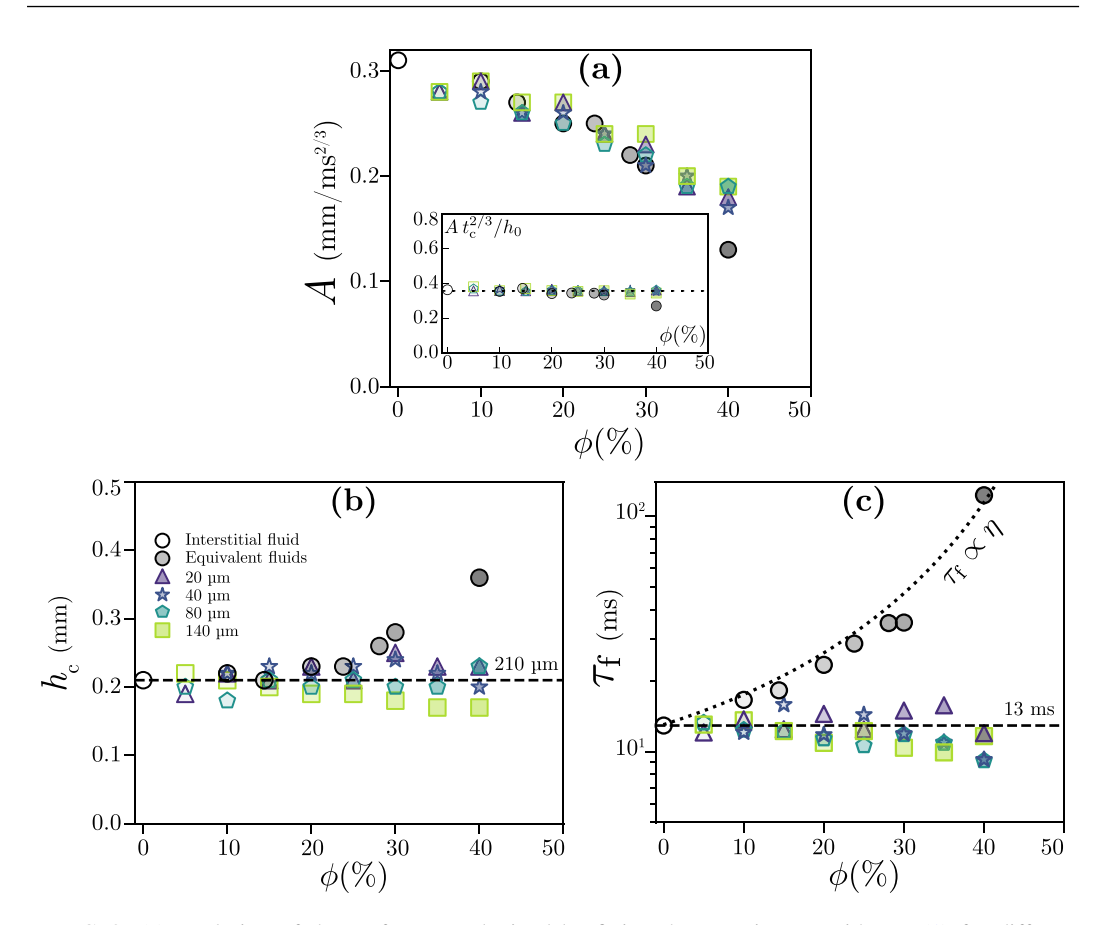


FIG. 3. (a) Evolution of the prefactor A obtained by fitting the experiments with Eq. (1) for different particle volume fractions ϕ . Inset: Dimensionless $A t_{\rm c}^{2/3}/h_0$ [Eq. (3)]. (b) Neck thickness at the transition to the viscoelastic regime $h_{\rm c}$ vs the volume fraction ϕ . (c) Relaxation time $\tau_{\rm f}$ vs particle volume fraction ϕ . The dotted line is the best fit for $\tau_{\rm f} \propto \eta$. Colored symbols represent different particle diameters, and gray circles denote the equivalent fluids plotted according to the equivalent particle fraction $\phi_{\rm eq}$.

fluid viscosity. Therefore, the main effect of the particles in the Newtonian regime is to increase the viscosity of the fluid.

The main difference with the pinch-off of a Newtonian fluid is that at $t=t_c$, the diameter of the liquid neck has a finite value. We define the critical thickness at the transition: $h_c=h_{\min}(t_c)$ [Fig. 2(a)]. Figure 3(b) reports the variations of h_c when increasing the volume fraction ϕ for different particle sizes. Surprisingly, we do not observe any significant effect of particles. The critical thickness h_c keeps an average value of $210 \pm 30~\mu m$ for all suspensions. This result is counterintuitive since h_c is typically of the order of magnitude of the size of the 140- μm particles. This is explicitly visible in Fig 1(c): First, at the scale of the neck, the suspension is no longer a continuous medium, and second, the large particles deform the free surface at the neck. However, it appears that these phenomena do not affect the value of h_c . If we now consider the equivalent viscous fluids, we observe that increasing the viscosity of the fluid leads to a thicker thickness at the transition. Again, although suspensions are more viscous than the interstitial liquid—ten times for $\phi=40\%$ —this does not play a role on h_c .

Similarly to h_c , the relaxation time τ_f is overall unaffected by the particles in the viscoelastic regime. Figure 3(c) reports that in the range of parameters considered here, there is no influence of the particle size nor of the volume fraction on τ_f , which average value equals 13 ms. However, for

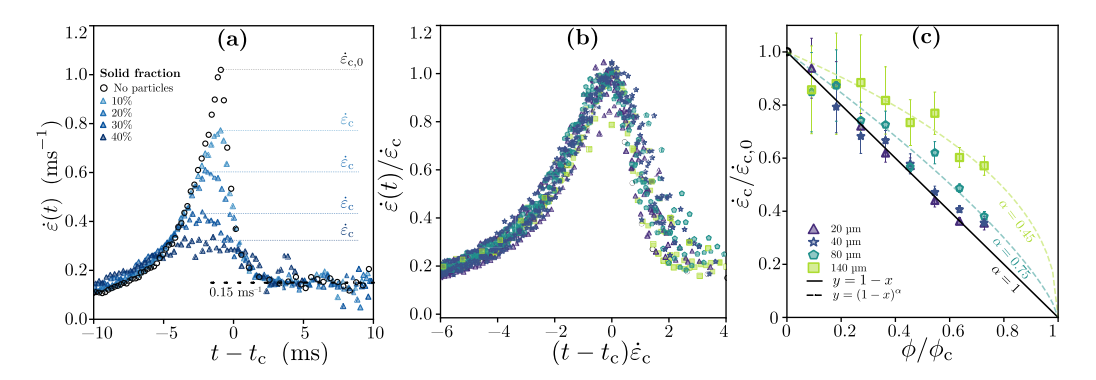


FIG. 4. (a) Time evolution of the strain rate at the neck $\dot{\varepsilon}$ for volume fractions ranging from $\phi=10\%$ (light blue) to $\phi=40\%$ (dark blue) of 20- μ m particles and for the interstitial viscoelastic fluid only (open circles). (b) Evolution of $\dot{\varepsilon}$ rescaled by the critical strain rate $\dot{\varepsilon}_c$ as a function of the rescaled time around the transition $(t-t_c)\dot{\varepsilon}_c$ for all particle diameters and volume fractions. (c) Critical strain rate of the viscoelastic suspensions $\dot{\varepsilon}_c$ normalized by that of the interstitial fluid $\dot{\varepsilon}_{c,0}$ as a function of ϕ/ϕ_c . The black line represents Eq. (6) for $\alpha=1$, and the dashed curves Eq. (6) with the value of α that best fits a given particle size.

the equivalent fluids, τ_f increases with the viscosity of the solvent [48]. The dotted line represents the best fit for a linear relation between τ_f and the viscosity and matches the behavior of the equivalent fluids. The absence of effects of the particles on h_c and τ_f implies that the dynamic is controlled by the stretching and the relaxation of the polymer chains, whose characteristic time scale is proportional to the solvent viscosity [49]. Then, at and after the transition, the bulk viscosity of the suspension is irrelevant. Even unwound, polymer chains remain small compared to the particles, typically of the order a few hundred of nanometers [48]. Therefore, at the scale of the polymer chains, the viscosity is that of the interstitial fluid η_0 and not the effective viscosity of the suspension. Hence, once the polymer chains are unwound, the thinning regime is only governed by the interstitial fluid, and the particles stop influencing the process.

We now consider the transition from the Newtonian regime to the viscoelastic regime. Rather than quantifying the thinning in terms of the neck width h_{\min} , we define the instantaneous strain rate at the neck, $\dot{\varepsilon} = (\partial v_z/\partial z)_{h_{\min}}$. Using the continuity equation, we obtain

$$\dot{\varepsilon} = -\frac{2}{h_{\min}} \frac{\partial h_{\min}}{\partial t}.$$
 (4)

Figure 4(a) shows that $\dot{\varepsilon}$ sharply increases up to a maximum value $\dot{\varepsilon}_c$ at the transition, and then decreases. The good agreement between $h_{\min}(t)$ and the exponential law given by Eq. (2) [Fig. 2(a)] shows that $\dot{\varepsilon}$ becomes constant and equal to $2/\tau_f \simeq 0.15~\mathrm{ms}^{-1}$ in the viscoelastic regime. Therefore, the Weissenberg number of the flow, Wi = $\lambda_0 \dot{\varepsilon}$, eventually equals 2/3, as reported in the literature [47]. The effect of particles dispersed in the viscoelastic interstitial liquid is twofold: When the volume fraction ϕ increases, the critical strain rate $\dot{\varepsilon}_c$ decreases, and the transition between the two regimes takes place over a longer time. These two effects have the same origin since $1/\dot{\varepsilon}_c$ is also the relevant timescale of the transition. Rescaling the strain rate as $\dot{\varepsilon}/\dot{\varepsilon}_c$ and the time as $(t-t_c)\dot{\varepsilon}_c$ shows that all experiments collapse on a single master curve [Fig. 4(b)]. This result demonstrates that the strain rate follows a self-similar dynamics around the transition, which is only controlled by the critical strain rate $\dot{\varepsilon}_c$.

To characterize the variations of $\dot{\varepsilon}_c$, we may consider that with rigid particles, the deformation of a volume of suspension is concentrated in its liquid phase. Hence, the local strain rate $\dot{\varepsilon}_{loc}$ is larger than the global strain rate $\dot{\varepsilon}$. Let us consider a single particle and the liquid around it, which is submitted to an external deformation $\dot{\varepsilon}$. In the nondimensionalized space, the particle occupies the volume ϕ and can move freely within the volume ϕ_c without encountering its neighbors. For

the suspensions considered here, the maximum packing fraction ϕ_c , that is, the volume fraction at which all particles are in contact so that the lubrication films between them vanish [18], is close to 55% [37]. This value is smaller than the random *close* packing fraction of 64% at which spheres maximize the number of their contact and where friction prevails over viscosity. However, it agrees with the recent results of Château *et al.* [37], who used similar particles but dispersed in a Newtonian liquid. Assuming infinitely rigid particles and an incompressible liquid, the deformation is entirely supported by the liquid. Since the liquid occupies the volume $\phi_c - \phi$, one can write $(\phi_c - \phi)\dot{\varepsilon}_{loc} = \phi_c\dot{\varepsilon}$. This approach considers the ideal case of an infinitely large volume where the particle do not feel the boundaries. In order to describe the confinement effects due to the geometry of the neck, we add a geometrical parameter α . We can then write the expression of the local strain rate in the liquid phase:

$$\dot{\varepsilon}_{\text{loc}} = \dot{\varepsilon} (1 - \phi/\phi_{\text{c}})^{-\alpha}. \tag{5}$$

We now consider the microscopic interactions between particles and polymer chains. The transition to the viscoelastic thinning regime corresponds to the coil-stretch transition of the polymer chains [40], which unwind when the strain rate of the solution reaches the critical value $\dot{\epsilon}_{c,0} \sim 1/2\tau_z$ [49]. The Zimm relaxation time, $\tau_z \sim \eta_0 R_g^3/(k_BT)$, is the relaxation time of the coiled polymer chain, with R_g its radius of gyration. Therefore, if we assume that the polymer chains between particles experience the local strain rate corresponding to Eq. (5), it means that for $\phi > 0$ the coil-stretch transition occurs when $\dot{\epsilon}_{loc} = \dot{\epsilon}_{c,0}$, although $\dot{\epsilon}_c < \dot{\epsilon}_{c,0}$. $\dot{\epsilon}_{c,0}$ can be measured directly in the case $\phi = 0$, and we obtain

$$\dot{\varepsilon}_{c} = \dot{\varepsilon}_{c,0} (1 - \phi/\phi_{c})^{\alpha}. \tag{6}$$

Figure 4(c) reports the ratio $\dot{\varepsilon}_{\rm c}/\dot{\varepsilon}_{\rm c,0}$ as a function of the volume fraction ϕ for different particle diameters. For particles up to 40 μ m the experiments are captured by the simplest version of Eq. (6) where $\alpha=1$. For larger particles, the value of α that best fits the data decreases: $\alpha=0.75$ for $d=80~\mu{\rm m}$ and $\alpha=0.45$ for $d=140~\mu{\rm m}$. Since we expect α to describe the geometry of the flow at the neck, it should only depend on the ratio of the two length scales present in the system: the width of the neck at the transition $h_{\rm c}$ and the diameter of the particles d. We expect α to be a function of $d/h_{\rm c}$, such that $\alpha\to 1$ for $d\ll h_{\rm c}$ and $\alpha\to 0$ for $d\gg h_{\rm c}$. Figure 4(c) shows that for $d\simeq h_{\rm c}$, we measure a value of $\dot{\varepsilon}_{\rm loc}$ that is greater than expected. In that case, at the scale of the particles, the liquid phase is bounded by the particles but also by the free surface [Fig 1(c)]. This confinement reduces the space around which the particles can move, and probably changes the local strain rate. However, this effect of confinement is only a supposition and deserves further studies.

In conclusion, we have characterized the effect of solid spherical particles on the thinning of viscoelastic dilute polymer solutions. By comparing the viscoelastic suspensions with equivalent fluids having the same shear viscosity, we have demonstrated that particles only affect the Newtonian regime by increasing the shear viscosity. We found that the viscoelastic thinning regime is not affected by particles and only controlled by the interstitial fluid. However, particles drastically change the transition from the Newtonian to the viscoelastic regime. As the neck thins down, the strain rate $\dot{\varepsilon}$ in the suspension increases. Because particles are rigid, coiled polymer chains between them experience a local strain rate $\dot{\varepsilon}_{loc}$, which is larger than $\dot{\varepsilon}$. When $\dot{\varepsilon}_{loc}$ becomes comparable to the Zimm relaxation time τ_z , the chains unwind and the flow becomes viscoelastic. Around the transition, $\dot{\varepsilon}$ follows a self-similar dynamic whose relevant scale is the critical strain rate $\dot{\varepsilon}_c$. If the particle size is comparable to that of the neck ($d \simeq h_c$), confinement effects make the motion of the particles more constrained, which increases the value of $\dot{\varepsilon}_c$. The output of this study goes beyond the pinch-off of viscoelastic suspensions as this model experiment enables a direct measurement of the local strain rate in the liquid phase of a granular suspension, a great challenge in the rheology of suspensions [18].

This material is based upon work supported by the National Science Foundation under NSF Faculty Early Career Development (CAREER) Program Award CBET No. 1944844. We thank B. Keshavarz for helpful discussions and comments.

- [1] E. Villermaux, Fragmentation, Annu. Rev. Fluid Mech. 39, 419 (2007).
- [2] B. Keshavarz, E. C. Houze, J. R. Moore, M. R. Koerner, and G. H. McKinley, Ligament Mediated Fragmentation of Viscoelastic Liquids, Phys. Rev. Lett. 117, 154502 (2016).
- [3] S. Kooij, R. Sijs, M. M. Denn, E. Villermaux, and D. Bonn, What Determines the Drop Size in Sprays? Phys. Rev. X 8, 031019 (2018).
- [4] E. Villermaux, Fragmentation versus cohesion, J. Fluid Mech. 898, P1 (2020).
- [5] B. Derby, Inkjet printing of functional and structural materials: Fluid property requirements, feature stability, and resolution, Annu. Rev. Mater. Res. 40, 395 (2010).
- [6] S. V. Murphy and A. Atala, 3D bioprinting of tissues and organs, Nat. Biotechnol. 32, 773 (2014).
- [7] K. B. Hatzell, M. B. Dixit, S. A. Berlinger, and A. Z. Weber, Understanding inks for porous-electrode formation, J. Mater. Chem. A 5, 20527 (2017).
- [8] E. Turkoz, A. Perazzo, H. Kim, H. A. Stone, and C. B. Arnold, Impulsively Induced Jets from Viscoelastic Films for High-Resolution Printing, Phys. Rev. Lett. 120, 074501 (2018).
- [9] W. C. K. Poon, A. T. Brown, S. O. L. Direito, D. J. M. Hodgson, L. Le Nagard, A. Lips, C. E. MacPhee, D. Marenduzzo, J. R. Royer, A. F. Silva *et al.*, Soft matter science and the COVID-19 pandemic, Soft Matter 16, 8310 (2020).
- [10] L. Bourouiba, The fluid dynamics of disease transmission, Annu. Rev. Fluid Mech. 53, 473 (2021).
- [11] S. Banerjee, R. Tripathy, D. Cozzens, T. Nagy, S. Keki, M. Zsuga, and R. Faust, Photoinduced smart, self-healing polymer sealant for photovoltaics, ACS Appl. Mater. Interfaces 7, 2064 (2015).
- [12] J. Eggers, Universal Pinching of 3D Axisymmetric Free-Surface Flow, Phys. Rev. Lett. 71, 3458 (1993).
- [13] C. Wagner, Y. Amarouchene, D. Bonn, and J. Eggers, Droplet Detachment and Satellite Bead Formation in Viscoelastic Fluids, Phys. Rev. Lett. 95, 164504 (2005).
- [14] P. P. Bhat, S. Appathurai, M. T. Harris, M. Pasquali, G. H. McKinley, and O. A. Basaran, Formation of beads-on-a-string structures during break-up of viscoelastic filaments, Nat. Phys. 6, 625 (2010).
- [15] B. Keshavarz, Nonlinear dynamics of complex fluids in fragmentation and fracture, Ph.D. thesis, Massachusetts Institute of Technology, 2017.
- [16] H. Y. Lo, Y. Liu, S. Y. Mak, Z. Xu, Y. Chao, K. J. Li, H. C. Shum, and L. Xu, Diffusion-Dominated Pinch-Off of Ultralow Surface Tension Fluids, Phys. Rev. Lett. 123, 134501 (2019).
- [17] F. Boyer, É. Guazzelli, and O. Pouliquen, Unifying Suspension and Granular Rheology, Phys. Rev. Lett. 107, 188301 (2011).
- [18] É. Guazzelli and O. Pouliquen, Rheology of dense granular suspensions, J. Fluid Mech. 852, P1 (2018).
- [19] C. Bonnoit, J. Lanuza, A. Lindner, and E. Clement, Mesoscopic Length Scale Controls the Rheology of Dense Suspensions, Phys. Rev. Lett. 105, 108302 (2010).
- [20] P. Peyla and C. Verdier, New confinement effects on the viscosity of suspensions, Europhys. Lett. 94, 44001 (2011).
- [21] C. E. Colosqui, J. F. Morris, and H. A. Stone, Hydrodynamically Driven Colloidal Assembly in Dip Coating, Phys. Rev. Lett. 110, 188302 (2013).
- [22] A. Gans, E. Dressaire, B. Colnet, G. Saingier, M. Z. Bazant, and A. Sauret, Dip-coating of suspensions, Soft Matter 15, 252 (2019).
- [23] A. Sauret, A. Gans, B. Colnet, G. Saingier, M. Z. Bazant, and E. Dressaire, Capillary filtering of particles during dip coating, Phys. Rev. Fluids 4, 054303 (2019).
- [24] B. M. Dincau, M. Z. Bazant, E. Dressaire, and A. Sauret, Capillary Sorting of Particles by Dip Coating, Phys. Rev. Appl. 12, 011001(R) (2019).
- [25] S. Palma and H. Lhuissier, Dip-coating with a particulate suspension, J. Fluid Mech. 869, R3 (2019).
- [26] P. S. Raux, A. Troger, P. Jop, and A. Sauret, Spreading and fragmentation of particle-laden liquid sheets, Phys. Rev. Fluids 5, 044004 (2020).
- [27] B. M. Dincau, E. Mai, Q. Magdelaine, J. A. Lee, M. Z. Bazant, and A. Sauret, Entrainment of particles during the withdrawal of a fibre from a dilute suspension, J. Fluid Mech. 903, A38 (2020).
- [28] D.-H. Jeong, A. Kvasnickova, J.-B. Boutin, D. Cébron, and A. Sauret, Deposition of a particle-laden film on the inner wall of a tube, Phys. Rev. Fluids 5, 114004 (2020).
- [29] D. A. Abdourahman, A. Geniere, M. Auriol, F. Dalas, A.-L. Biance, and M. Le Merrer, Generation and stability of cement soap films, Soft Matter 17, 2429 (2021).

- [30] R. J. Furbank and J. F. Morris, An experimental study of particle effects on drop formation, Phys. Fluids **16**, 1777 (2004).
- [31] M. Z. Miskin and H. M. Jaeger, Droplet formation and scaling in dense suspensions, Proc. Natl. Acad. Sci. USA 109, 4389 (2012).
- [32] C. Bonnoit, T. Bertrand, E. Clément, and A. Lindner, Accelerated drop detachment in granular suspensions, Phys. Fluids 24, 043304 (2012).
- [33] T. Bertrand, C. Bonnoit, E. Clément, and A. Lindner, Dynamics of drop formation in granular suspensions: The role of volume fraction, Granular Matter 14, 169 (2012).
- [34] M. S. van Deen, T. Bertrand, N. Vu, D. Quéré, E. Clément, and A. Lindner, Particles accelerate the detachment of viscous liquids, Rheol. Acta 52, 403 (2013).
- [35] W. Mathues, C. McIlroy, O. G. Harlen, and C. Clasen, Capillary breakup of suspensions near pinch-off, Phys. Fluids 27, 093301 (2015).
- [36] V. Thiévenaz, S. Rajesh, and A. Sauret, Droplet detachment and pinch-off of bidisperse particulate suspensions, Soft Matter, (2021), doi: 10.1039/D1SM00593F.
- [37] J. Château, É. Guazzelli, and H. Lhuissier, Pinch-off of a viscous suspension thread, J. Fluid Mech. 852, 178 (2018).
- [38] G. H. McKinley and T. Sridhar, Filament-stretching rheometry of complex fluids, Annu. Rev. Fluid Mech. 34, 375 (2002).
- [39] B. Keshavarz, V. Sharma, E. C. Houze, M. R. Koerner, J. R. Moore, P. M. Cotts, P. Threlfall-Holmes, and G. H. McKinley, Studying the effects of elongational properties on atomization of weakly viscoelastic solutions using Rayleigh Ohnesorge jetting extensional rheometry (ROJER), J. Non-Newtonian Fluid Mech. 222, 171 (2015).
- [40] Y. Amarouchene, D. Bonn, J. Meunier, and H. Kellay, Inhibition of the Finite-Time Singularity During Droplet Fission of a Polymeric Fluid, Phys. Rev. Lett. **86**, 3558 (2001).
- [41] J. Eggers and E. Villermaux, Physics of liquid jets, Rep. Prog. Phys. 71, 036601 (2008).
- [42] E. Turkoz, J. M. Lopez-Herrera, J. Eggers, C. B. Arnold, and L. Deike, Axisymmetric simulation of viscoelastic filament thinning with the Oldroyd-B model, J. Fluid Mech. 851, R2 (2018).
- [43] A. Deblais, M. A. Herrada, J. Eggers, and D. Bonn, Self-similarity in the breakup of very dilute viscoelastic solutions, J. Fluid Mech. 904, R2 (2020).
- [44] See Supplemental Material at http://link.aps.org/supplemental/10.1103/PhysRevFluids.6.L062301 for the videos corresponding to Fig. 1 and a more detailed experimental description.
- [45] A. Deblais, K. P. Velikov, and D. Bonn, Pearling Instabilities of a Viscoelastic Thread, Phys. Rev. Lett. 120, 194501 (2018).
- [46] J. B. Keller and M. J. Miksis, Surface tension driven flows, SIAM J. Appl. Math. 43, 268 (1983).
- [47] S. L. Anna and G. H. McKinley, Elasto-capillary thinning and breakup of model elastic liquids, J. Rheol. 45, 115 (2001).
- [48] L. E. Rodd, J. J. Cooper-White, D. V. Boger, and G. H. McKinley, Role of the elasticity number in the entry flow of dilute polymer solutions in micro-fabricated contraction geometries, J. Non-Newtonian Fluid Mech. 143, 170 (2007).
- [49] P. G. De Gennes, Coil-stretch transition of dilute flexible polymers under ultrahigh velocity gradients, J. Chem. Phys. **60**, 5030 (1974).